The Astrophysical Journal Letters, 947:L33 (7pp), 2023 April 20 https://doi.org/10.3847/2041-8213/accb9f

Unusual Martian Foreshock Waves Triggered by a Solar Wind Stream Interaction Region

Zhenpeng Su[1,2,3], Yuming Wang[1,2,3], Tielong Zhang[4,5], Zhiyong Wu[1,2,3], Long Cheng[1,2,3], Zhuxuan Zou[1,2,3], Chenglong Shen[1,2,3], Jingnan Guo[1,2,3], Sudong Xiao[4], Guoqiang Wang[4], Zonghao Pan[1,2,3], Kai Liu[1,2,3], Xinjun Hao[1,2,3], Yiren Li[1,2,3], Manming Chen[1,2,3], Yutian Chi[1,2,3], and Mengjiao Xu[1,2,3]

[1] Deep Space Exploration Laboratory/School of Earth and Space Sciences, University of Science and Technology of China, Hefei 230026, People's Republic of China; szpe@mail.ustc.edu.cn, ymwang@ustc.edu.cn
[2] CAS Center for Excellence in Comparative Planetology/CAS Key Laboratory of Geospace Environment/Mengcheng National Geophysical Observatory, University of Science and Technology of China, Hefei 230026, People's Republic of China
[3] Collaborative Innovation Center of Astronautical Science and Technology, Hefei 230026, People's Republic of China
[4] Institute of Space Science and Applied Technology, Harbin Institute of Technology, Shenzhen 518000, People's Republic of China
[5] Space Research Institute, Austrian Academy of Sciences, A-8042 Graz, Austria
Received 2023 March 11; revised 2023 April 6; accepted 2023 April 9; published 2023 April 25

Abstract

Planetary bow shocks noncollisionally dissipate the incident bulk flow energy of solar wind into some other forms. To what extent and how solar wind disturbances affect the energy dissipation processes at the bow shocks on different planets remain unclear. With the Chinese Tianwen-1 and American Mars Atmosphere and Volatile EvolutioN missions, we present the first observation of significant modifications by a solar wind stream interaction region to the Martian foreshock waves, which are an important energy dissipation product of the bow shock. After the stream interface hitting Mars, an unusual band of foreshock waves emerged, with a central frequency of ∼0.4 Hz and frequency width of ∼0.2 Hz. These waves exhibited highly distorted waveforms, with peak-to-peak amplitudes of 10–25 nT in contrast to a background magnetic field of 6–9 nT. They were approximately elliptically polarized with respect to the wavevector and propagated highly obliquely to the background magnetic field. These waves reported here differed greatly from the commonly known Martian foreshock "30 s waves" and "1 Hz waves," but resembled, to some extent, the less frequently occurring terrestrial foreshock "3 s waves." Our present findings may imply an unexpected energy dissipation pattern of the Martian bow shock to the disturbed solar wind, which needs further observational, theoretical, and numerical investigations.

Unified Astronomy Thesaurus concepts: Planetary bow shocks (1246); Solar-planetary interactions (1472); Corotating streams (314); Space weather (2037); Space plasmas (1544); Plasma physics (2089)

1. Introduction

Collisionless plasma shocks commonly occur throughout the heliosphere and beyond. How these shocks noncollisionally dissipate the incident bulk flow energy has been a fundamental question in space and astrophysics (Lembege et al. 2004; Wilson 2016). In the heliospheric solar wind, there exist transient structures (e.g., coronal mass ejections and stream interaction regions), discontinuities (e.g., shocks, and rotational and tangential discontinuities), and turbulence of various scales. To what extent and how solar wind disturbances affect the energy dissipation processes at the bow shocks on different planets remain unclear.

With in situ measurements since the 1960s, foreshock waves have been considered an important energy dissipation product of the terrestrial bow shock (Russell & Hoppe 1983; Eastwood et al. 2005; Wilson et al. 2014). There are phenomenally six terrestrial foreshock wave or structure types in the low-frequency range of the spacecraft frame: (1) "30 s waves" (e.g., Fairfield 1969), typically with periods of ∼30 s, normal angles of 10°–40°, and linear, left- or right-hand polarizations; (2) "10 s waves" (e.g., Hoppe & Russell 1983; Eastwood et al. 2003), typically with periods of ∼10 s, normal angles of 7°–53° and right-hand polarizations; (3) "3 s waves" (e.g., Russell et al. 1971; Le et al. 1992), typically with periods near 3 s, normal angles below 20°, and right-hand polarizations; (4) "1 Hz waves" (e.g., Fairfield 1974), typically with frequencies close to 1 Hz, normal angles 20°–70°, and left- or right-hand polarizations; (5) shocklets (e.g., Hoppe et al. 1981), characteristically appearing as small shock-like magnetic pulsations; (6) short large-amplitude magnetic structures (e.g., Schwartz et al. 1992), characteristically appearing as localized, irregular magnetic pulsations. These wave types defined above by the period or frequency are based on the terrestrial foreshock observations. For a specified foreshock wave type, its frequency may be different in the different planetary scenarios. A 30 s wave, for instance, has a similar frequency at both the Earth (e.g., Eastwood et al. 2005) and Venus (e.g., Shan et al. 2016), but it is distinct significantly from that at Mercury (e.g., Le et al. 2013). Compared with Earth, Mars is generally immersed in the solar wind of lower density and weaker magnetic field. Meanwhile, different from Earth, Mars lacks a global intrinsic magnetic field and its magnetosphere arises from the direct interaction between solar wind and atmosphere. Beyond the Martian shock, there exist neutral oxygen and hydrogen exospheres from photochemical and thermal processes (Anderson & Hord 1971; Feldman et al. 2011). Since the 1990s, in situ measurements (Brain et al. 2002; Dubinin & Fraenz 2016; Ruhunusiri et al. 2016; Collinson et al. 2018; Halekas et al. 2020) have revealed the Martian counterparts to

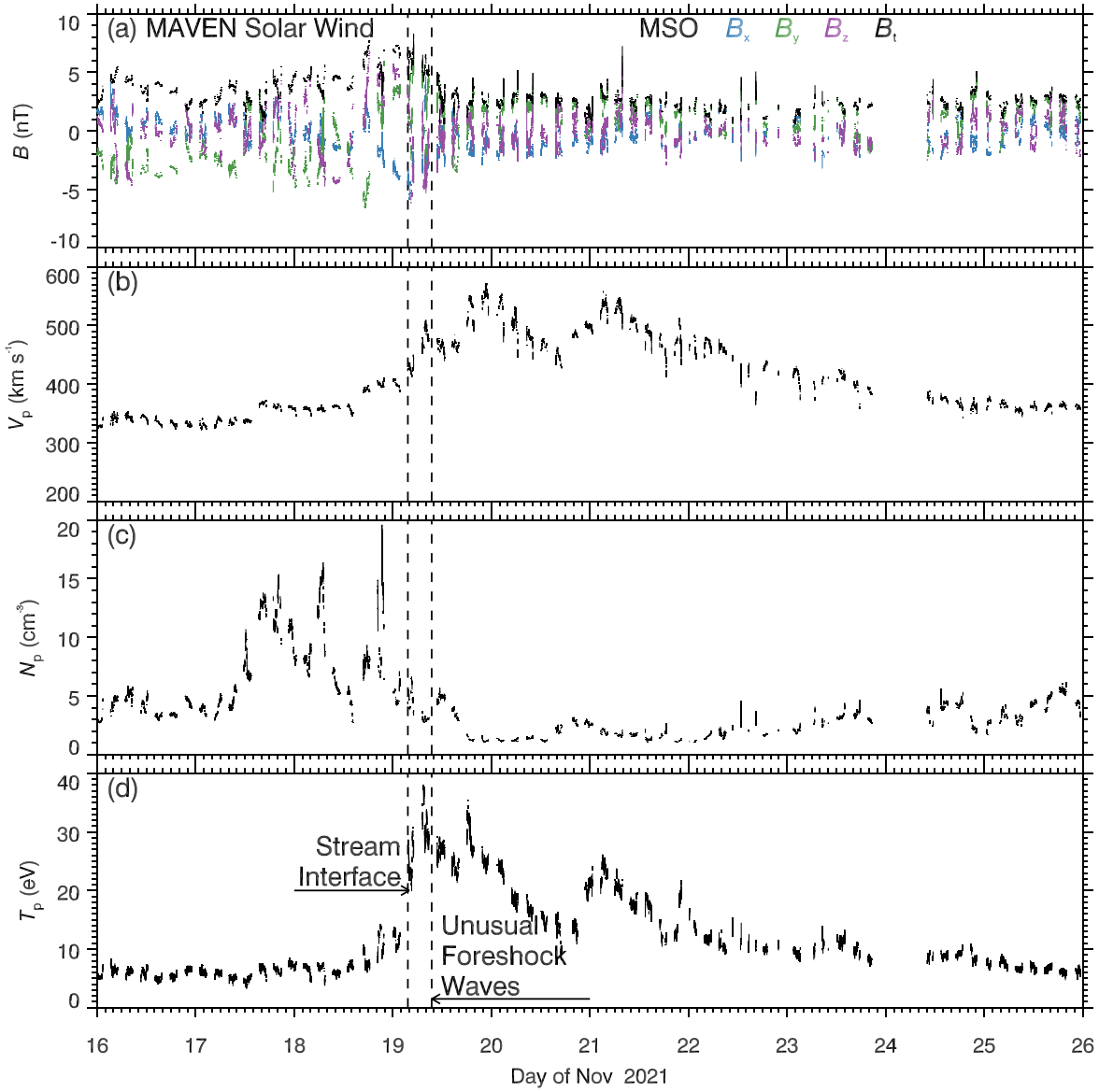

Figure 1. Overview of solar wind upstream of Martian bow shock. (a) Magnetic field components (B_x, B_y, B_z) and magnitude B_t in the Mars-centered Solar Orbital (MSO) coordinate system. (b)–(d) Proton velocity V_p, density N_p, and temperature T_p. The two vertical dashed lines mark the time points around which the solar stream interface and the unusual foreshock waves occurred.

terrestrial foreshock waves and structures: 30 s waves, 1 Hz waves, shocklets, and short large-amplitude magnetic structures.

In this Letter, we will concentrate on the impact of large-scale solar wind transients on planetary foreshock waves. However, the required experimental test is quite challenging, because of the very limited time of planets immersed in the solar wind transients and the only sporadic measurements near the planetary bow shocks. With the Cluster mission (Escoubet et al. 2001) at Earth, Turc et al. (2019) showed that, in response to interplanetary magnetic clouds, the usually quasi-monochromatic terrestrial foreshock waves were replaced by a superposition of waves at different frequencies. Here we report an experimental test of the significant modification of Martian foreshock waves by a solar wind stream interaction region, serendipitously made with Tianwen-1 (Wan et al. 2020) and Mars Atmosphere and Volatile EvolutioN (MAVEN; Jakosky et al. 2015) missions.

2. Observation

The Chinese first Mars mission Tianwen-1 entered the Mars orbit in 2021 February. The Mars Orbiter Magnetometer (Liu et al. 2020) of Tianwen-1 started measuring on 2021 November 15 (Wang et al. 2023) and detected the unusual foreshock waves on 2021 November 19. The Tianwen-1 spacecraft was in an elliptical orbit with a periapsis altitude of ∼270 km and apoapsis altitude of ∼11,000 km. During the period of interest, Tianwen-1 was able to take approximately 4 hr to measure the solar wind within each orbital period of ∼7 hr. In the same time window, the MAVEN spacecraft was orbiting Mars with a periapsis altitude of ∼170 km and apoapsis altitude of ∼4400 km. Within each orbital period of ∼3.5 hr, MAVEN was able to take approximately 1.5 hr to measure the solar wind. Our present analysis involves data of magnetic field $\boldsymbol{B}$ and solar wind proton velocity $\boldsymbol{V}_p$, density N_p and temperature T_p provided by the Magnetometer (Connerney et al. 2015a) and

Solar Wind Ion Analyzer (Halekas et al. 2015) on board MAVEN.

Figure 1 shows an overview of background solar wind measured by MAVEN during 2021 November 16–26. We extract these measurements with the following criteria: $V_p > 310$ km s^{-1}, 1 cm^{-3} $< N_p <$ 20 cm^{-3}, and $T_p < 40$ eV, and then filter the data oscillations near the bow shock. Clearly, a solar wind stream interaction region had hit Mars. The slow and fast streams had velocities of 350 km s^{-1} and 550 km s^{-1}, and their interface with clear jump variations in velocity, density, and temperature (Burlaga 1974) occurred at approximately 03:40 UT on 2021 November 19. Around the stream interface, the compressed magnetic fields $\boldsymbol{B}$ fluctuated significantly. Approximately 6 hr later than the stream interface, Tianwen-1 magnetometer detected the unusual foreshock waves.

Figure 2 presents Tianwen-1's magnetometer measurements during the outbound pass from 09:11 UT to 09:41 UT on 2021 November 19. The major axis of Tianwen-1's elliptical orbit lay on the southeast flank of Mars in the Mars-centered Solar Orbital (MSO) coordinate system (Figure 2(a)). We identify the specific spatial regions from the behaviors of magnetic fields with a sampling rate of 1 Hz (Figure 2(b)): the bow shock characterized as a boundary with jump variations of the magnetic field components and magnitudes around 09:29 UT, the magnetosheath with the turbulent magnetic fields, and the upstream solar wind with the relatively weak magnetic fields. As shown in Figure 2(a), the identified shock position was close to the model prediction of Trotignon et al. (2006). Applying the minimum variance analysis (Sonnerup & Cahill 1967) to magnetic fields near the bow shock and approximating the shock normal to be parallel to the minimum varying component, we estimate the angle between shock normal and upstream unperturbed magnetic field to be $\theta_S = 74°$. We apply the wavelet transform (Torrence & Compo 1998) to the magnetic fields with a sampling rate of 32 Hz, define the mean magnetic fields by a 10 s running-average of the instantaneous magnetic fields, and obtain the compressional (Figure 2(c)) and transverse (Figure 2(d)) magnetic power spectrograms. From the shock ramp (09:28 UT) to upstream (09:39 UT) of the bow shock, there was a band of strong waves in the frequency range of 0.25–0.60 Hz. Their transverse power were slightly higher than the compressional power. Along with the southward movement of Tianwen-1 by 0.4 R_M (R_M is the Mars radii) within 11 minutes, the central frequency of observed foreshock waves appeared to rise systematically from 0.3 to 0.5 Hz. Around 09:39 UT, a jump variation of the magnetic field caused the foreshock waves to disappear suddenly.

In Figures 3(a)–(c), we show three representative segments of foreshock waveforms with a sampling rate of 32 Hz. The waveforms are obtained by subtracting the mean values from the instantaneous magnetic fields in the MSO coordinate system. They exhibited periodic nonsinusoidal fluctuations with large amplitudes. With the background magnetic field $B_0 = 6$–9 nT, the peak-to-peak amplitude ΔB of waves ranged from 10 to 25 nT. The waves with $\Delta B \approx 10$ nT around 09:34:13 UT appeared to be a superposition of multiple monochromatic sinusoidal waves. Higher ΔB apparently corresponded to more distorted waveforms (with shock-like, sawtooth-like, bipolar-like, or soliton-like patterns). We bandpass filter the waveform of Figure 3(c) in a period range of 0.5–10 s, and then perform the minimum variance analysis to the bandpass waveform (Figures 3(d) and (e)). We approximate the wavevector to be parallel or antiparallel to the minimum varying direction $\boldsymbol{N}_W = (0.80, -0.60, 0.14)$. Given the averaged background magnetic field vector $\boldsymbol{B}_0 = (-2.11, 0.86, -5.07)$ nT, we estimate the wave normal angle to be $\psi_W = 58.^{\circ}6$ (with a 180° ambiguity). During the 16 s interval, the normal component was generally at a low level of ±2 nT. There was a clear trend of a right-hand elliptical polarization with respect to the estimated wave normal direction $\boldsymbol{N}_W$, although the polarization trajectories were highly distorted.

3. Conclusion and Discussion

With the very recent Tianwen-1 mission and the MAVEN mission in orbit for more than 8 yr, we experimentally test the influence of a solar wind stream interaction region on the Martian foreshock waves. MAVEN monitored the stream interaction region hitting Mars during 2021 November 16–26, and Tianwen-1 happened to detect an unusual band of waves during its outbound crossing of the quasi-perpendicular ($\theta_S = 74°$) bow shock on 2021 November 19.

The foreshock waves reported here differed greatly from the previously mentioned Martian foreshock waves in frequency, amplitude, and waveform pattern. The frequencies of 1 Hz waves (Brain et al. 2002) statistically have a lower quartile of 0.5 Hz and an upper quartile of 0.8 Hz. The frequencies of 30 s waves (Ruhunusiri et al. 2016) are below the proton gyrofrequency. For both waves, their frequencies are usually stable in a specific event. In the frequency–time spectrogram, our newly reported waves appeared as a narrow band with a drifting frequency from 0.3 to 0.5 Hz (approximately 2–5 times the proton gyrofrequency). These newly reported waves had peak-to-peak amplitudes of 10–25 nT, approximately 5–10 times larger than those of 1 Hz waves and 30 s waves (Brain et al. 2002; Connerney et al. 2015b; Ruhunusiri et al. 2016). In contrast to the quasi-monochromatic sinusoidal waveforms of 1 Hz waves and 30 s waves (Brain et al. 2002; Connerney et al. 2015b; Ruhunusiri et al. 2016; Halekas et al. 2020), our newly reported waves had highly distorted waveforms. The wave band reported here could be composed of multiple monochromatic waves. As the wave amplitudes grew to a sufficiently high level, their waveforms could be deformed nonlinearly (e.g., Shan et al. 2020).

The Martian foreshock waves reported here roughly fell in the same frequency range as the terrestrial 3 s waves (Le et al. 1992). A subset of terrestrial 3 s waves have the irregular waveforms with peak-to-peak amplitudes up to 10 nT (Blanco-Cano et al. 1999), resembling to some extent the Martian foreshock waves reported here. The terrestrial 3 s waves have a quite low occurrence rate (Le et al. 1992; Burgess 1997; Blanco-Cano et al. 1999; Hobara et al. 2007; Wang et al. 2021). As shown in the most recent statistical studies (Wang et al. 2021) on the basis of the Magnetospheric Multiscale mission, the terrestrial 3 s waves are observed on average six times per month. This newly reported Martian foreshock wave type does not occur often either. Closely before and after Tianwen-1 crossing of the bow shock, MAVEN did not detect any foreshock waves (Figure 4). Note that the shock normal angles were 88.3° and 13.6° during the inbound and outbound passes of MAVEN. In fact, such Martian foreshock waves were recorded only once in the freshly released database of Tianwen-1 from 2021 November 15 to December 31.

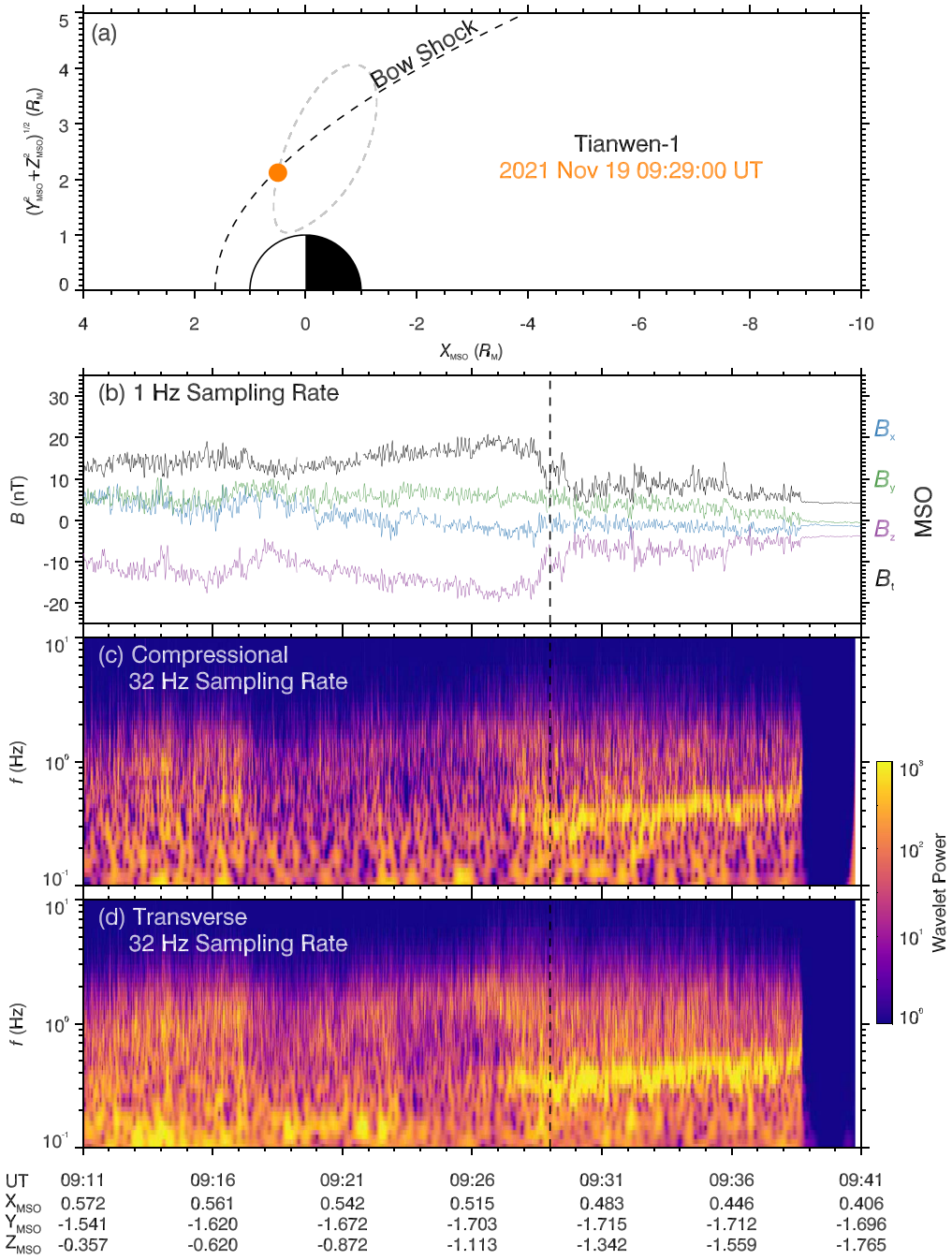

Figure 2. Unusual Martian foreshock waves observed by Tianwen-1. (a) Empirical bow-shock configuration (Trotignon et al. 2006; black dashed line) and Tianwen-1's orbit (gray dashed line) and bow-shock crossing point (orange dot) in the X_{MSO}–$\sqrt{Y^2_{MSO}+Z^2_{MSO}}$ plane. (b) Magnetic field components (B_x, B_y, B_z) and magnitude B_t with a 1 Hz sampling rate in the MSO coordinate system. (c) and (d) Compressional and transverse magnetic power spectral densities (color-coded) from the wavelet transform of the magnetic fields with a sampling rate of 32 Hz.

The solar wind stream interaction region is rich in discontinuities and turbulence of various scales (Crooker et al. 1999) and evolves with distance (Huang et al. 2019; Telloni et al. 2021). These discontinuities and turbulence could significantly affect the energy dissipation of the bow shock (Kropotina et al. 2021; Trotta et al. 2022). Near Earth, both 30 s waves and 3 s waves could be driven by the beam instabilities (Gary 1991) of backstreaming ions from the bow shock. Turc et al. (2019) showed that, in response to interplanetary magnetic clouds, the usually quasi-monochromatic terrestrial foreshock waves were replaced by a superposition of waves at different frequencies. In contrast to a single ion beam for the quasi-monochromatic foreshock waves, multiple ion beams were found for the concurrence of multiple waves (Turc et al. 2019). By analogy, we speculate that, for the event reported here, the stream interaction region could change the amount and intensity of backstreaming ion beams from the Martian bow shock and then cause the superposition and deformation of foreshock waves. The observed foreshock wave frequency drift over a timescale of 11 minutes and spatial scale of 0.4 R_M (Figures 2(c) and (d)) could result from the variations in the characteristic parameters of either the solar wind or

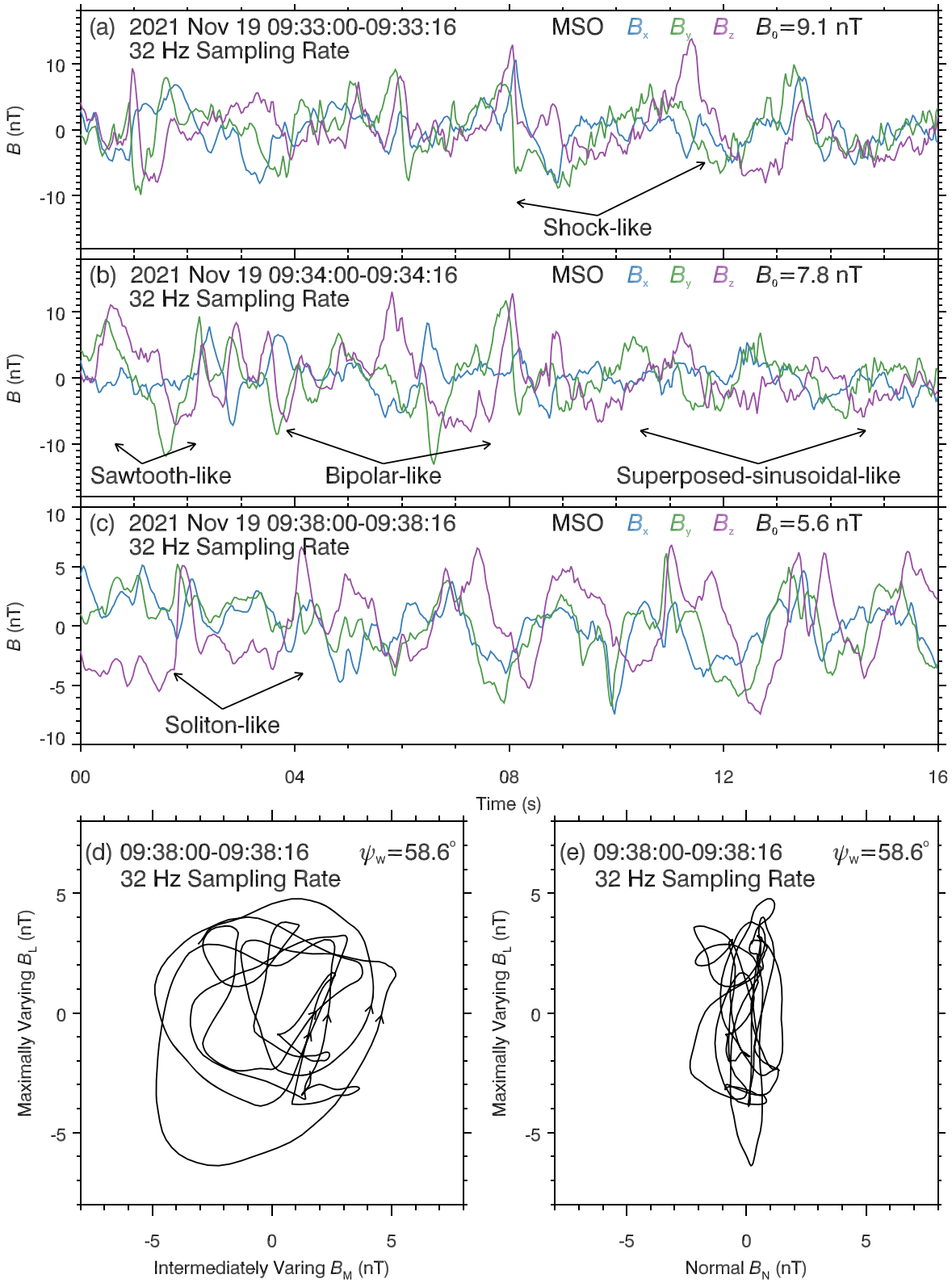

Figure 3. Martian foreshock wave properties. (a)–(c) Three representative segments of waveforms in the MSO coordinate system. Colors help differentiate among three magnetic field components. (d) and (e) Hodogram of bandpass waveform on the basis of minimum variance analysis.

backstreaming ion beams or both. For example, Blanco-Cano et al. (1999) suggested that backstreaming ion beams with higher densities allowed the linear growth rates of right-hand instabilities to peak at higher frequencies in the plasma frame. Inside the solar wind stream interaction region, both magnetic fields and particles were temporally variable. The change of incident solar wind would modify the backstreaming ion beam characteristics. Meanwhile, because of the ongoing wave–particle interactions, the backstreaming ion beam characteristics might evolve with distance away from the bow shock. To

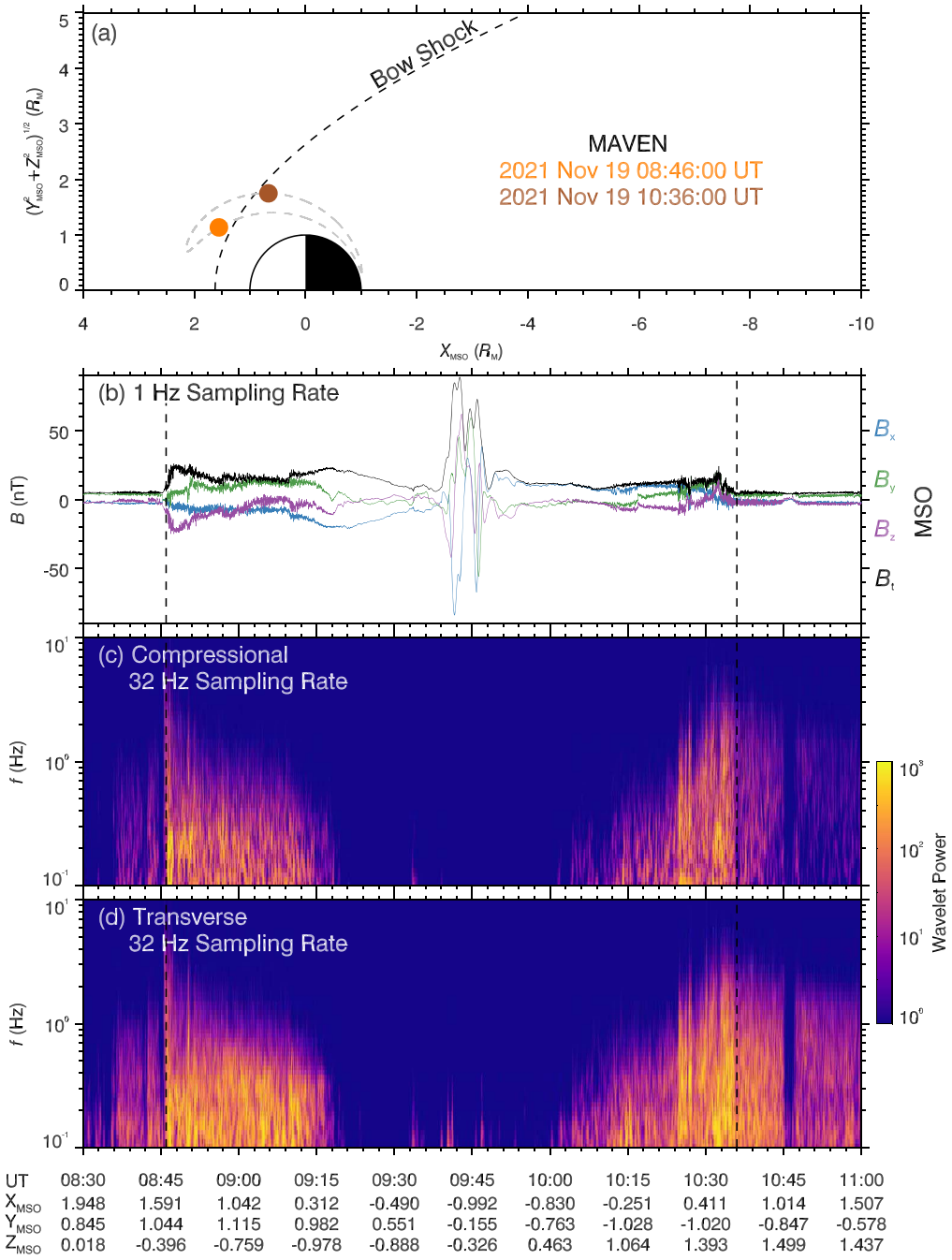

Figure 4. The same format as Figure 2, except for MAVEN with two bow-shock crossing points over a longer time period.

validate the hypotheses above requires the simultaneous particle measurements. Unfortunately, the Mars Ion and Neutral Particle Analyzer (Kong & Zhang et al. 2020; Fan et al. 2022; Zhang & Kong et al. 2022) on board Tianwen-1 was not working during this event. In future, more observational, theoretical, and numerical works are required to understand the planetary bow-shock dynamics (including wave generation and damping as well as particle heating and acceleration) modified by various solar wind disturbances.

We acknowledge the entire Tianwen-1 and MAVEN teams for providing data. Tianwen-1 data may be applied at CNSA Data Release System (http://202.106.152.98:8081/marsdata/) or downloaded from the official website of the MOMAG team (http://space.ustc.edu.cn/dreams/tw1_momag/). MAVEN data were available from the website (https://lasp.colorado.edu/maven/sdc/public/data/sci/) or the NASA Planetary Data System (http://doi.org/10.17189/1414178 for the MAVEN MAG Calibrated Data Bundle and http://doi.org/10.17189/1414182 for the MAVEN SWIA Calibrated Data Bundle). This work was supported by the National Natural Science Foundation of China grants 42130204, 42188101, 42274198, and 42074222, the Strategic Priority Research Program of Chinese Academy of Sciences grant XDB 41000000, and the Key Research Program of the Chinese Academy of Sciences grant ZDRE-KT-2021-3.

ORCID iDs

Zhenpeng Su https://orcid.org/0000-0001-5577-4538
Yuming Wang https://orcid.org/0000-0002-8887-3919
Long Cheng https://orcid.org/0000-0003-0578-6244
Zhuxuan Zou https://orcid.org/0009-0008-9920-9600
Chenglong Shen https://orcid.org/0000-0002-3577-5223
Guoqiang Wang https://orcid.org/0000-0002-6618-4928
Kai Liu https://orcid.org/0000-0003-2573-1531
Yutian Chi https://orcid.org/0000-0001-9315-4487
Mengjiao Xu https://orcid.org/0000-0002-2924-7520

References

Anderson, D. E., & Hord, C. W. 1971, JGR, 76, 6666
Blanco-Cano, X., Le, G., & Russell, C. T. 1999, JGRA, 104, 4643
Brain, D. A., Bagenal, F., Acuña, M. H., et al. 2002, JGRA, 107, 1076
Burgess, D. 1997, AdSpR, 20, 673
Burlaga, L. F. 1974, JGR, 79, 3717
Collinson, G., Wilson, L. B., Omidi, N., et al. 2018, JGRA, 123, 7241
Connerney, J. E. P., Espley, J., Lawton, P., et al. 2015a, SSRv, 195, 257
Connerney, J. E. P., Espley, J. R., DiBraccio, G. A., et al. 2015b, GeoRL, 42, 8819
Crooker, N. U., Gosling, J. T., Bothmer, V., et al. 1999, SSRv, 89, 179
Dubinin, E., & Fraenz, M. 2016, in Low-Frequency Waves in Space Plasmas, ed. A. Keiling, D.-H. Lee, & V. Nakariakov (Hoboken, NJ: Wiley), 343
Eastwood, J. P., Balogh, A., Lucek, E. A., Mazelle, C., & Dandouras, I. 2003, AnGeo, 21, 1457
Eastwood, J. P., Balogh, A., Lucek, E. A., Mazelle, C., & Dandouras, I. 2005, JGR, 110, A11219
Eastwood, J. P., Lucek, E. A., Mazelle, C., et al. 2005, SSRv, 118, 41
Escoubet, C. P., Fehringer, M., & Goldstein, M. 2001, AnGeo, 19, 1197
Fairfield, D. H. 1969, JGR, 74, 3541
Fairfield, D. H. 1974, JGR, 79, 1368
Fan, K., Yan, L., Wei, Y., et al. 2022, ScChD, 65, 759
Feldman, P. D., Steffl, A. J., Parker, J. W., et al. 2011, Icar, 214, 394
Gary, S. 1991, SSRv, 56, 373–415
Halekas, J. S., Ruhunusiri, S., Vaisberg, O. L., et al. 2020, JGRA, 125, e2020JA028221
Halekas, J. S., Taylor, E. R., Dalton, G., et al. 2015, SSRv, 195, 125
Hobara, Y., Walker, S. N., Balikhin, M., et al. 2007, JGRA, 112, A07202
Hoppe, M. M., & Russell, C. T. 1983, JGR, 88, 2021
Hoppe, M. M., Russell, C. T., Frank, L. A., Eastman, T. E., & Greenstadt, E. W. 1981, JGRA, 86, 4471
Huang, H., Guo, J., Wang, Z., et al. 2019, ApJ, 879, 118
Jakosky, B. M., Lin, R. P., Grebowsky, J. M., et al. 2015, SSRv, 195, 3
Kong, L., Zhang, A., et al. 2020, E&PP, 4, 1
Kropotina, J. A., Webster, L., Artemyev, A. V., et al. 2021, ApJ, 913, 142
Le, G., Chi, P. J., Blanco-Cano, X., et al. 2013, JGRA, 118, 2809
Le, G., Russell, C. T., Thomsen, M. F., & Gosling, J. T. 1992, JGRA, 97, 2917
Lembege, B., Giacalone, J., Scholer, M., et al. 2004, SSRv, 110, 161
Liu, K., Hao, X., Li, Y., et al. 2020, E&PP, 4, 384
Ruhunusiri, S., Halekas, J. S., Connerney, J. E. P., et al. 2016, JGRA, 121, 2374
Russell, C. T., Childers, D. D., & Coleman, P. J. 1971, JGR, 76, 845
Russell, C. T., & Hoppe, M. M. 1983, SSRv, 34, 155
Schwartz, S. J., Burgess, D., Wilkinson, W. P., et al. 1992, JGR, 97, 4209
Shan, L., Du, A., Tsurutani, B. T., et al. 2020, ApJL, 888, L17
Shan, L., Mazelle, C., Meziane, K., et al. 2016, JGRA, 121, 7385
Sonnerup, B. U. O., & Cahill, L. J. J. 1967, JGR, 72, 171
Telloni, D., Sorriso-Valvo, L., Woodham, L. D., et al. 2021, ApJL, 912, L21
Torrence, C., & Compo, G. P. 1998, BAMS, 79, 61
Trotignon, J., Mazelle, C., Bertucci, C., & Acuña, M. 2006, P&SS, 54, 357
Trotta, D., Pecora, F., Settino, A., et al. 2022, ApJ, 933, 167
Turc, L., Roberts, O. W., Archer, M. O., et al. 2019, GeoRL, 46, 12644
Wan, W. X., Wang, C., Li, C. L., & Wei, Y. 2020, NatAs, 4, 721
Wang, S., Chen, L.-J., Ng, J., et al. 2021, PhPl, 28, 082901
Wang, Y., Zhang, T., Wang, G., et al. 2023, E&PP, 7, 1
Wilson, L. B. 2016, GMS, 216, 269
Wilson, L. B., Sibeck, D. G., Breneman, A. W., et al. 2014, JGRA, 119, 6475
Zhang, A., Kong, L., et al. 2022, E&PP, 6, 1